AIAA JOURNAL
Vol. 44, No. 12, December 2006

Technical Notes

TECHNICAL NOTES are short manuscripts describing new developments or important results of a preliminary nature. These Notes should not exceed 2500 words (where a figure or table counts as 200 words). Following informal review by the Editors, they may be published within a few months of the date of receipt. Style requirements are the same as for regular contributions (see inside back cover).

Synthetic Jet Flowfield Database for Computational Fluid Dynamics Validation

Chungsheng Yao,* Fang Jenq Chen,* and Dan Neuhart*
NASA Langley Research Center, Hampton, Virginia 23681

DOI: 10.2514/1.13819

Introduction

A workshop on computational fluid dynamics (CFD) validation of synthetic jets and turbulent separation control† was held at the NASA Langley Research Center in 2004 to assess the current CFD capability to predict an unsteady flowfield. Three selected test cases were 1) a basic flowfield generated by a synthetic jet in a quiescent environment, 2) a round oscillatory jet in a crossflow, and 3) the control of separated flow over a wall-mounted hump model.

This paper describes the flowfield database for case 1. Flowfield measurements were obtained using three different techniques: particle image velocimetry (PIV), laser Doppler velocimetry (LDV), and hot-wire anemometry. In addition, the actuator operating parameters, including diaphragm displacement, internal cavity pressure, and internal cavity temperature, were documented to provide boundary conditions for CFD modeling.

Among active flow control devices being developed, synthetic jets have demonstrated promising flow control applications [1]. Considerable studies have covered the development of the actuator and the general behavior of the synthetic jets. However, there has not been a complete data set to support the validation of CFD prediction of synthetic jets.

Smith and Glezer [2] measured the velocity profile of plane jets from rectangular slots with hot-wire and flow visualization. Crook et al. [3] studied the development of a round jet using an analytical model and compared their results with hot-wire measurements. Mallinson et al. [4] studied a round jet with variable orifice diameters and cavity heights using a hot wire. Chen et al. [5] provided velocity profiles at the centerline of a plane jet, and jet exit velocity profiles with a hot wire. Muller et al. [6] used PIV to measure the detailed flowfield of a circular jet. Bera et al. [7] used PIV to map plane synthetic jet flows from a 2-D slot. Guy et al. [8] studied a plane synthetic jet with hot-wire measurements.

This study was not intended to be a parametric survey or performance optimization of synthetic jets.

Presented as Paper 2218 at the 2nd AIAA Flow Control Conference, Portland, OR, 24 June–1 July 2004; received 7 October 2004; revision received 28 February 2006; accepted for publication 24 April 2006.

*Aerospace Engineer, Flow Physics and Control Branch, MS 170.

†Data available on-line at http://cfdval2004.larc.nasa.gov [cited March 2004].

Experiment Setup

The synthetic jet actuator contained a single pumping cavity in line with the jet exit slot (Fig. 1). The exit slot is 1.25 mm wide (h) and 33.6 mm long. The flow coordinates are shown in Fig. 2. The actuator was flush-mounted on an aluminum plate with a glass enclosure (610 mm each side).

The jet was driven by a single piezoelectric diaphragm (50.8 mm in diameter) mounted on one side of the cavity. The diaphragm was driven at 445 Hz, a frequency selected for stability and repeatability. The cavity resonant frequency was 450 Hz.

Three actuator parameters, diaphragm displacement d, cavity pressure p, and cavity temperature T, were measured to monitor the actuator performance and to provide the boundary conditions for CFD modeling. A fiber optics displacement sensor measured the diaphragm displacement at the center of the piezoelectric diaphragm. A dynamic pressure transducer was installed at the center of the sidewall to monitor the cavity pressure. A thermocouple device was installed at the bottom of the cavity to monitor the internal temperature (Fig. 3).

Flowfield Measurement

Hot-wire measurements were made with a constant-temperature anemometer (CTA) using a single-wire probe. The sensing element was 5 mm in diameter and 1.25 mm long, operated at an overheat ratio of 1.8. The probe was mounted perpendicular to the floor with the sensing element located at the center of the slot and parallel to the axis of the slot. Measurements were taken at 47 stations from slot exit to 50 mm above.

Nonlinearized signals from the CTA outputs were sampled at 100 kHz with 16,384 data points recorded at each station, corresponding to about 72 periods of the driving frequency. Each period contained 225 data points. Seventy-two periods were averaged to compute the phase-averaged statistics. Hot-wire signals were derectified to obtain negative velocities during the suction cycle at lower stations. Derectification follows the phase of driving signals. Uncertainty was $\pm 2.5\%$ for measurements at heights of 5 mm or higher and $\pm 6\%$ for stations near the solid surface.

A LDV system was set up to measure the vertical jet velocity along the centerline of the slot ($x = 0, y = 0$). Velocity measurements were made at 47 stations between 0 and 70 mm above the slot. The seeding particles were polystyrene latex spheres 0.9 μm in diameter with specific gravity at 1.04. From a first-order estimation, particles $\sim\mathcal{O}$ (1 μm) followed the flow well at the applied frequency. The cross-beam half angle was 1.872 deg, calibrated at the far field. The focal length for LDV optics was 750.5 mm. The sample volume was about 175 μm. LDV signals were processed using Fast Fourier Transform processors based on a 256 point spectrum analysis.

Thirty thousand data points were collected at each station and sorted into 36 phase bins, at 10 deg phase interval. The number of samples within each bin ranged from hundreds to over 2000. These samples were used to compute phase-averaged statistics. The total uncertainty was estimated to be ± 0.54 m/s.

A digital PIV system was set up to measure the horizontal and vertical velocity components synchronized with the drive signal. The PIV system included 1024×1280 pixel CCD cameras installed with 200 mm and 105 mm lenses for large and near flowfield measurements, respectively, corresponding to 9 and 30 mm fields of view. Imaging optics was calibrated with an optical target aligned

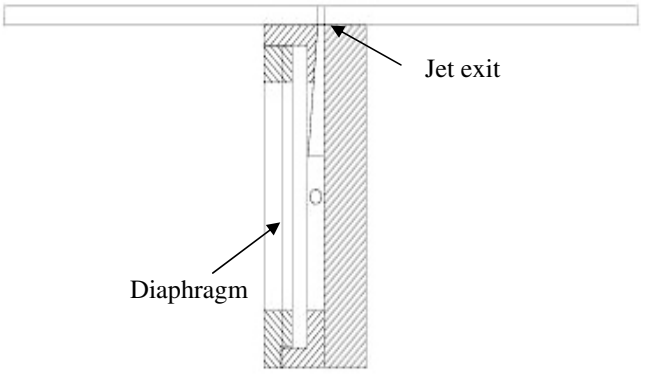

Fig. 1 Schematic diagram of the cavity (side view).

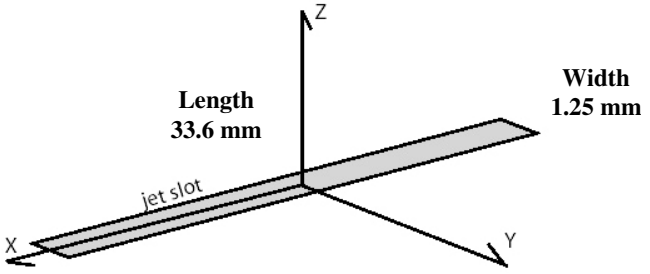

Fig. 2 Synthetic jet coordinates.

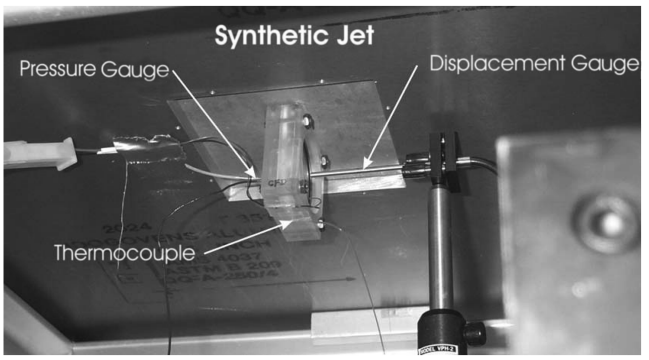

Fig. 3 Synthetic actuator and sensors for pressure, displacement, and temperature.

with the laser sheet. The calibration accuracy was within ± 1 pixel over 1240 pixels. Interrogation resolution was set between 28 to 32 pixels, corresponding to about 0.22 mm and 0.77 mm of measurement area for large and near field-of-view tests.

A laser light sheet, between 0.3 and 0.5 mm thick, was projected perpendicular to the slot at the midsection for y–z plane measurements, and parallel to the slot for x–z plane measurements. Laser pulses were adjusted to maximize the PIV performance. PIV interrogation resolves between $1/10$ to $1/20$ of subpixel resolution. This PIV system has been shown to measure within 1% of freestream velocity in wind tunnel tests.

Polydispersed smoke particles, with a specific gravity at 1.022 and a size distribution from submicron to tens of micron were used for seeding. Simple drag law analysis showed that particles less than 3 μm should have followed the oscillatory flow well.

A total of 72 phases were collected in 5 deg increments for PIV measurements across the slot. Along the slot, PIV samples at 18 phases in 20 deg phase increments. Individual PIV measurements collected 400 samples to compute the phase-averaged statistics. Convergence of estimation occurred between 100 and 200 samples. PIV data validation rate was near 100% overall. This might be reduced to 20% or lower inside vortex cores due to seeding absence.

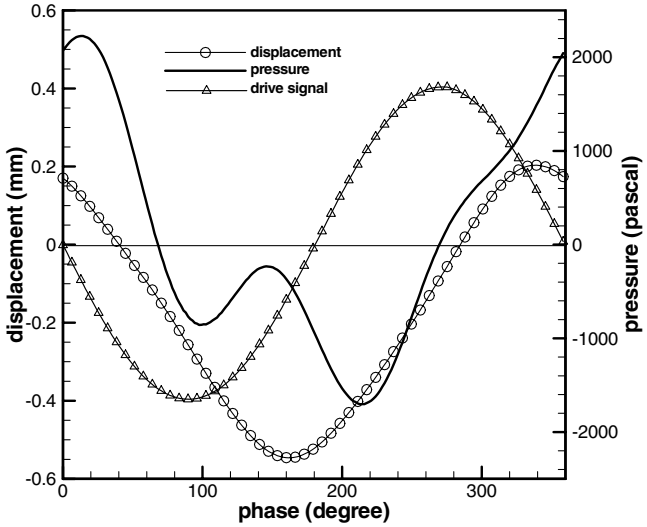

Fig. 4 Waveforms of drive signal (2.6 V, peak-to-peak), displacement, and cavity pressure.

Results

Environment

The cavity temperature stabilized at 6–7°C above the ambient air. The diaphragm displacement lagged behind the driver signal by 50–60 deg (Fig. 4). Pressure waveforms inside the cavity showed higher harmonics generated through the interior geometry. The higher harmonics might be of secondary effect to the synthetic jet, as both displacement and jet exit velocity displayed simple waveforms.

The square root of the peak pressure varied almost linearly with the diaphragm displacement (Fig. 5). Because the mass flux is proportional to the diaphragm displacement, the jet velocity may be scaled by either the displacement or the square root of the peak pressure.

Synthetic Jet Flowfield

The discussion of the synthetic jet flowfield is based on PIV measurements which covered three zones: 1) near field at x–z plane, (2) far field at x–z plane, and (3) y–z plane. The plane jet flow consists of a pulse train of high-speed fluid ejected from the slot accompanied by a pair of vortex rows developed about $0.5h$ above the slot. An elongated mean plane jet emerges when the flowfields are time- or ensemble-averaged over the driving cycle. Figure 6a shows the mean jet (streamwise) velocity contours at $x = 0$. The jet is a narrow and vertical near the exit. The jet turns into a wider and diffusive jet about

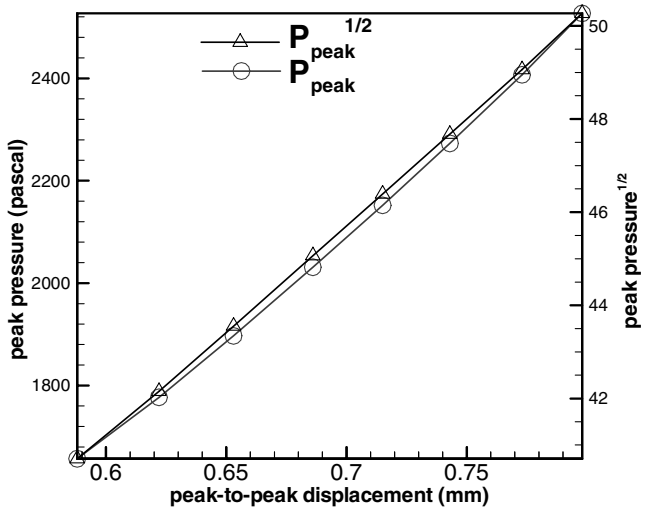

Fig. 5 Cavity pressure as function of diaphragm displacement.

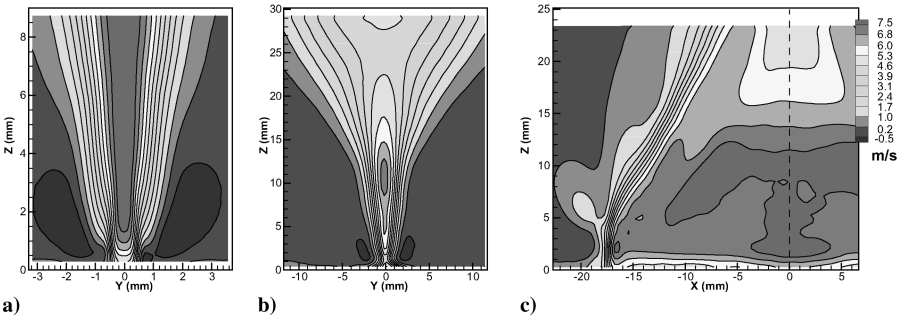

Fig. 6 Mean jet contours across the slot, a) close-up, b) large field, and c) parallel to slot.

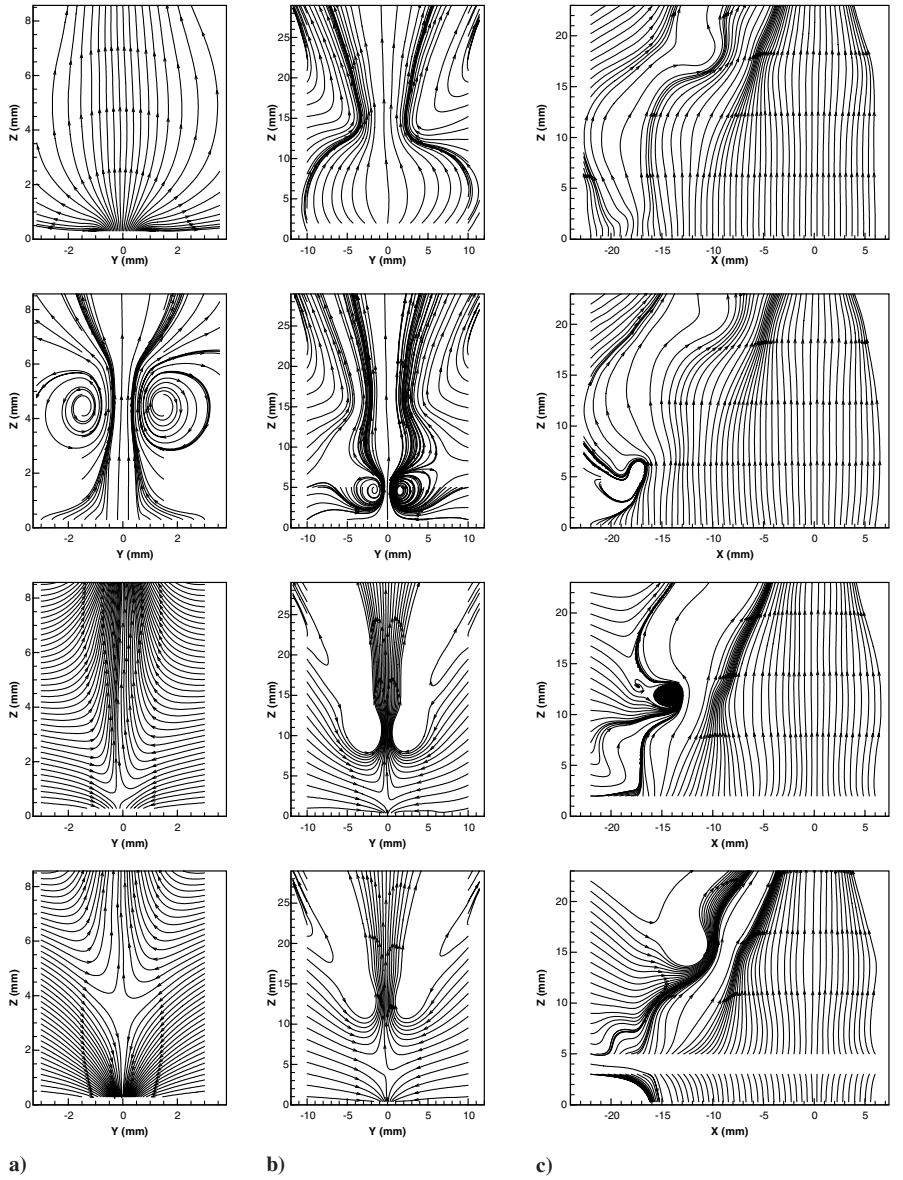

Fig. 7 Phase-averaged flowfield streamlines at phase 10, 100, 180, and 280 deg in a plane a) and b) across the slot, and c) parallel to slot.

$12h$ above the slot (Fig. 6b). The large field-of-view PIV does not properly resolve the high-speed jet core between Figs. 6a and 6b.

In the plane at $y = 0$, a more complicated plane jet structure is developed (Fig. 6c). The jet flow emanates uniformly near the jet exit. At about $4h$ height, the end vortices roll toward the center of the jet. The slant rolling of the end vortices may be connected to the wide jet spreading downstream in the x–z plane. Two-dimensional CFD modeling is therefore limited to the region within $8h$ distance from the jet exit.

Figure 7 presents four samples of phase-averaged synthetic jet flow fields from three fields of view. In first phase, the jet is beginning to emerge from the slot (top row) at the 10 deg phase (referenced to the input function). The remains of the prior jet mass at far field coexist in views 7b and 7c. At 100 deg, a pair of vortices moves with

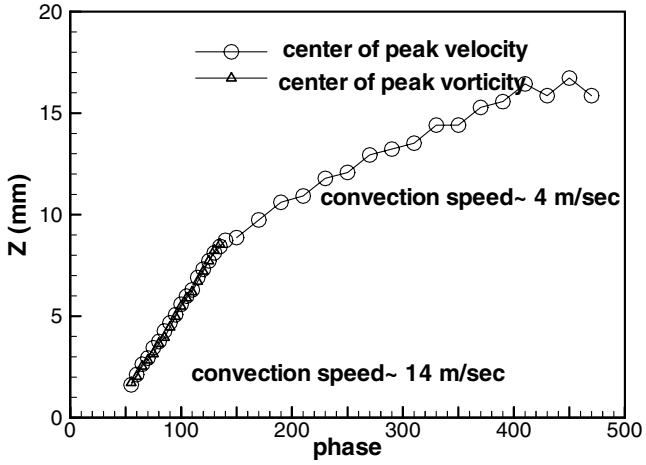

Fig. 8 Trajectories of jet and vortex.

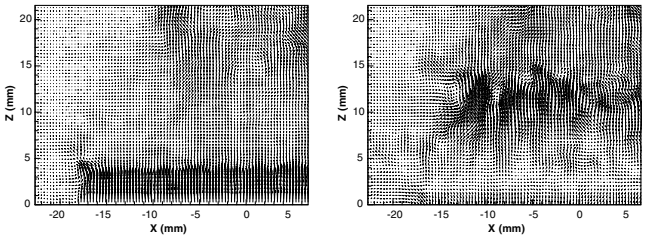

a) **b)**

Fig. 9 Instantaneous flowfield along the jet slot sampled at a) phase = 120 deg and b) phase = 180 deg.

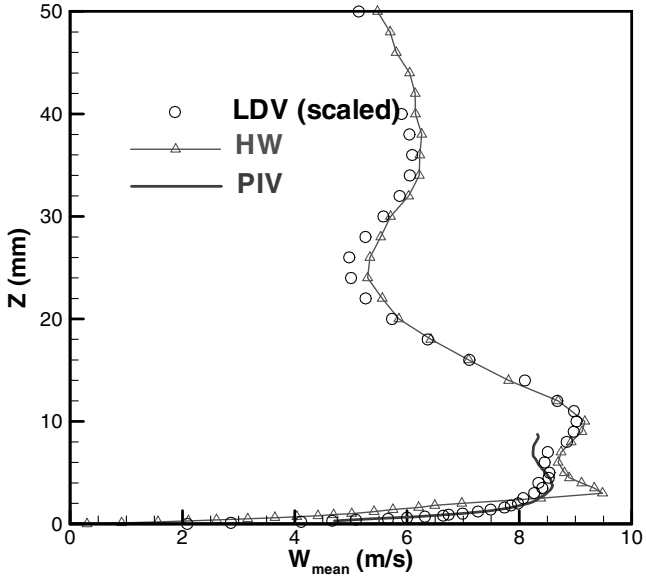

Fig. 10 Mean jet velocity profiles, averaged over one cycle.

the jet downstream. At 180 deg, the suction action controls the lower section near the slot, while the jet mass moves downstream. At 280 deg, the suction action extends upward but diminishes near $\sim 4h$ above the slot. From the side view, the plane jets show the growth of the edge vortex with height moving toward the center along with the jet fronts.

The jet convection velocity, or the rate of ascending, is estimated from the trajectory of the peak velocity and its phase (Fig. 8). Two convection speeds are estimated: 14 m/s in the near field and 4 m/s in the far field, displaying the two stages of the jet development. The vortex pair convects at the same velocity with the jet. In the first stage,

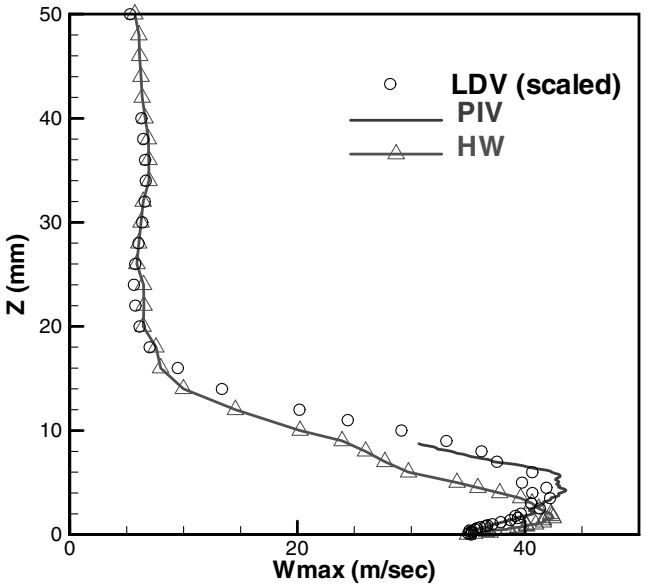

Fig. 11 Maximum jet velocity profiles.

the convection speed is less than the jet maximum velocity ($\sim$40 m/s). Therefore, the jet flow may be from the induced motion of the vortex pair in the near field. Downstream, the vortex expands and weakens; the jet mean, maximum, and convection velocity reduce to same level. The jet reaches its limit at about 12–13h. Beyond, the flowfield is quite diffused and stationary. Within the jet plane, secondary vortical structures develop as the jet moves downstream (Fig. 9).

Comparison Between Hot-Wire, LDV, and PIV

The mean velocity profiles from all three measurements at the center of the slot are shown in Fig. 10. LDV and PIV profiles show a close agreement. Because the LDV data were taken inadvertently at a higher displacement amplitude, the LDV data were scaled by amplitude to match the PIV profile. The hot-wire data show lower means near the exit, then agree with LDV and PIV data at higher stations. The zigzag of the hot-wire profile takes place from signal derectification due to the flow reversal within a $4h$ distance from the jet exit.

The comparison of the maximum jet velocity profiles among hot-wire, LDV, and PIV is similar to the mean profile comparison. Maximum velocity refers to the peak velocity within the driving cycle at each measurement station along the jet axis. LDV and PIV profiles (Fig. 11) agree in general, but the magnitude is off. Rescaling the LDV profile by the displacement amplitude improves the agreement. Scaling the maximum velocity using (peak pressure)$^{1/2}$ is found to be equally effective. LDV and PIV measurements show that the maximum velocity in the jet increases with height to about $z \sim 4h(\sim 5$ mm). The hot-wire profile shows higher maximum near the exit. It peaks near $z \sim 1.5h(\sim 2$ mm) then decays fast. Downstream of $z > 15h(\sim 19$ mm), the agreement between the mean profiles from hot-wire and LDV data matches well. The maximum velocity increases slightly at $z \sim 28h(36$ mm). This minor reversal is also seen in the PIV mean in Fig. 9.

Examples of proper scaling on velocity phase history using displacement amplitude are shown in Fig. 12.

Summary

A detailed flowfield database of a synthetic jet flow in quiescent air is provided for the CFD validation including phase-averaged flow fields from PIV at planes normal and parallel to the jet, supplemented by actuator pressure, temperature, and diaphragm displacement. The plane jet starts with a two-dimensional uniform motion in the near field with vortex pairs parallel to the slot and vortex rings at both

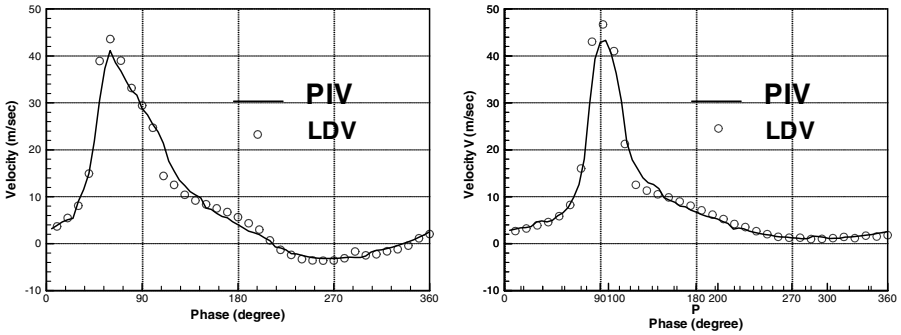

a) b)

Fig. 12 Comparison of scaled LDV velocity waveforms with PIV at two heights.

sides. Within the plane jet, the flow can be highly fluctuating as the jets advance, and the side vortex rings roll toward the center turning the jet to three-dimensional flow. There are two stages of jet development downstream, giving evidence of different flow processes in each stage. A 2-D modeling may only be sufficient or valid within the first stage of the jet development.

In the near field, close agreement is seen between the LDV and PIV when the jet velocity profiles are scaled by the peak cavity pressure or diaphragm displacement. Hot-wire measurements are off in comparison with LDV and PIV at lower stations, but the agreement improves downstream.

References

[1] Seifert, A., and Pack, L. G., "Active Control of Separated Flows on Generic Configurations at High Reynolds Number," AIAA Paper 99-3403, 1999.

[2] Smith, B. L., and Glezer, A., "The Formation and Evolution of Synthetic Jets," *Physics of Fluids*, Vol. 10, No. 9, 1998, pp. 2281–2297.

[3] Crook, A., Sadri, A. M., and Wood, N. J., "The Development and Implementation of Synthetic Jets for the Control of Separated Flow," AIAA Paper 99-33445, 1999.

[4] Mallinson, G., Hong, G., and Reizes, J. A., "Some Characteristics of Synthetic Jets," AIAA Paper 99-33673, 1999.

[5] Chen, F.-J., Yao, C., Beeler, G. B., Bryant. R. G., and Fox, R. L., "Development of Synthetic Jet Actuators for Active Flow Control at NASA Langley," AIAA Paper 2000-2405, 2000.

[6] Muller, M. O., Bernal, L. P., Miska, P. K., Washabaugh, P. D., Chou, T., Parviz, B., Zhang, C., and Najafi, K., "Flow Structure and Performance of Axisymmetric Synthetic Jets," AIAA Paper 2001-1008, 2001.

[7] Bera, J. C., Michard, M., Grosjean, N., and Comte-Bellot, G., "Flow Analysis of Two-Dimensional Pulsed Jets by Particle Image Velocimetry," *Experiments in Fluids*, Vol. 31, No. 5, 2001, pp 519–532.

[8] Guy, Y., McLaughlin, T. E., and Morrow, J. A., "Velocity Measurements in a Synthetic Jet," AIAA Paper 2001-16049, 2001.

T. Beutner
Associate Editor